Gene symbol	Description	Fold-change
CD22	Homo sapiens cDNA: FLJ22814 fis, clone KAIA3004, [AK026467]	1.12
NOV	Homo sapiens nephroblastoma overexpressed gene (NOV), mRNA [NM_002514]	1.12
ZNF554	Homo sapiens zinc finger protein 554 (ZNF554), mRNA [NM_001102631]	1.12
C5orf13	Homo sapiens chromosome 5 open reading frame 13 (C5orf13), transcript variant 1, mRNA [NM_004772]	1.11
YOD1	Homo sapiens YOD1 OTU deubiquinating enzyme 1 homolog (S. cerevisiae) (YOD1), mRNA [NM_018566]	1.11
IL23A	Homo sapiens interleukin 23, alpha subunit p19 (IL23A), mRNA [NM_016584]	1.11
FAM49A	Homo sapiens family with sequence similarity 49, member A (FAM49A), mRNA [NM_030797]	1.10
ZNF606	Homo sapiens zinc finger protein 606 (ZNF606), mRNA [NM_023927]	1.10
NCRNA00081	Homo sapiens non-protein coding RNA 81 (NCRNA00081), non-coding RNA [NR_002802]	1.10
ZMYND12	Homo sapiens zinc finger, MYND-type containing 12 (ZMYND12), mRNA [NM_032257]	1.10
ZNF596	Homo sapiens zinc finger protein 596 (ZNF596), transcript variant 1, mRNA [NM_001042416]	1.10
DNAJB9	Homo sapiens DnaJ (Hsp40) homolog, subfamily B, member 9 (DNAJB9), mRNA [NM_012328]	1.10
TRIM36	Homo sapiens tripartite motif-containing 36 (TRIM36), transcript variant 1, mRNA [NM_018700]	1.10
BAT4	Homo sapiens HLA-B associated transcript 4 (BAT4), mRNA [NM_033177]	1.10
AKAP12	Homo sapiens A kinase (PRKA) anchor protein 12 (AKAP12), transcript variant 2, mRNA [NM_144497]	1.10
RCOR1	Homo sapiens REST corepressor 1 (RCOR1), mRNA [NM_015156]	1.09
ZNF761	Homo sapiens zinc finger protein 761 (ZNF761), mRNA [NM_001008401]	1.09
RNF138	Homo sapiens ring finger protein 138 (RNF138), transcript variant 1, mRNA [NM_016271]	1.08
SLAMF7	Homo sapiens SLAM family member 7 (SLAMF7), mRNA [NM_021181]	1.08
SNX25	Homo sapiens sorting nexin 25 (SNX25), mRNA [NM_031953]	1.08
FYN	Homo sapiens FYN oncogene related to SRC, FGR, YES (FYN), transcript variant 1, mRNA [NM_002037]	1.08

ene symbol	Description	Fold-change
RB2	Homo sapiens adrenergic, beta-2-, receptor, surface (ADRB2), mRNA [NM_000024]	1.08
SP5	Homo sapiens dual specificity phosphatase 5 (DUSP5), mRNA [NM_004419]	1.08
RA3	Homo sapiens HtrA serine peptidase 3 (HTRA3), mRNA [NM_053044]	1.08
EKHA4	Homo sapiens pleckstrin homology domain containing, family A (phosphoinositide binding specific) member 4 (PLEKHA4), mRNA [NM_020904]	1.07
PI2	Homo sapiens tissue factor pathway inhibitor 2 (TFPI2), mRNA [NM_006528]	1.07
D3	Homo sapiens adducin 3 (gamma) (ADD3), transcript variant 1, mRNA [NM_016824]	1.07
NL2	Homo sapiens muscleblind-like 2 (Drosophila) (MBNL2), transcript variant 1, mRNA [NM_144778]	1.07
ED2	Homo sapiens Cbp/p300-interacting transactivator, with Glu/Asp-rich carboxy-terminal domain, 2 (CITED2), mRNA [NM_006079]	1.07
CS2	Homo sapiens suppressor of cytokine signaling 2 (SOCS2), mRNA [NM_003877]	1.07
F664	Homo sapiens zinc finger protein 664 (ZNF664), mRNA [NM_152437]	1.06
CR4	Homo sapiens chemokine (C-X-C motif) receptor 4 (CXCR4), transcript variant 1, mRNA [NM_001008540]	1.06
4-Mar	Homo sapiens membrane-associated ring finger (C3HC4) 4 (MARCH4), mRNA [NM_020814]	1.06
L26	Homo sapiens chemokine (C-C motif) ligand 26 (CCL26), mRNA [NM_006072]	1.06
1orf91	Homo sapiens chromosome 21 open reading frame 91 (C21orf91), transcript variant 2, mRNA [NM_017447]	1.06
NE1	Homo sapiens spectrin repeat containing, nuclear envelope 1 (SYNE1), transcript variant 2, mRNA [NM_033071]	1.05
ANXA1	Homo sapiens sperm protein associated with the nucleus, X-linked, family member A1 (SPANXA1), mRNA [NM_013453]	1.05
DN	Homo sapiens palladin homolog (mouse) (PLDN), mRNA [NM_012388]	1.05
RC58	Homo sapiens leucine rich repeat containing 58 (LRRC58), mRNA [NM_001099678]	1.05
ID5B	Homo sapiens AT rich interactive domain 5B (MRF1-like) (ARID5B), mRNA [NM_032199]	1.04

Gene symbol	Description	Fold-change
LOC643401	Homo sapiens hypothetical protein LOC340109, mRNA (cDNA clone IMAGE:5578073), partial cds [BC039509]	1.04
WBP5	Homo sapiens WW domain binding protein 5 (WBP5), transcript variant 1, mRNA [NM_016303]	1.04
TRIB1	Homo sapiens tribbles homolog 1 (Drosophila) (TRIB1), mRNA [NM_025195]	1.04
NT5E	Homo sapiens 5'-nucleotidase, ecto (CD73) (NT5E), mRNA [NM_002526]	1.04
DMBT1	Homo sapiens deleted in malignant brain tumors 1 (DMBT1), transcript variant 2, mRNA [NM_007329]	1.04
PAG1	Homo sapiens phosphoprotein associated with glycosphingolipid microdomains 1 (PAG1), mRNA [NM_018440]	1.04
PTPRH	Homo sapiens protein tyrosine phosphatase, receptor type, H (PTPRH), mRNA [NM_002842]	1.04
CSTA	Homo sapiens cystatin A (stefin A) (CSTA), mRNA [NM_005213]	1.04
LOC100132288	Homo sapiens cDNA clone IMAGE:5295205, with apparent retained intron. [BC043212]	1.04
THAP5	Homo sapiens THAP domain containing 5 (THAP5), transcript variant 2, mRNA [NM_152529]	1.04
DHDH	Homo sapiens dihydrodiol dehydrogenase (dimeric) (DHDH), mRNA [NM_014475]	1.03
TPD52	Homo sapiens tumor protein D52 (TPD52), transcript variant 1, mRNA [NM_001025252]	1.03
SPOCD1	Homo sapiens cDNA FLJ39908 fis, clone SPLEN2012620, [AK097227]	1.03
C1orf133	Homo sapiens chromosome 1 open reading frame 133 (C1orf133), non-coding RNA [NR_024337]	1.03
NR4A1	Homo sapiens nuclear receptor subfamily 4, group A, member 1 (NR4A1), transcript variant 1, mRNA [NM_002135]	1.03
ZNF302	Homo sapiens zinc finger protein 302 (ZNF302), transcript variant 1, mRNA [NM_018443]	1.03
KLHL23	Homo sapiens kelch-like 23 (Drosophila) (KLHL23), mRNA [NM_144711]	1.03
AADAC	Homo sapiens arylacetamide deacetylase (esterase) (AADAC), mRNA [NM_001086]	1.02
GAS5	Homo sapiens growth arrest-specific 5 (non-protein coding) (GAS5), non-coding RNA [NR_002578]	1.02

Gene symbol	Description	Fold-change
C17orf91	Homo sapiens chromosome 17 open reading frame 91 (C17orf91), transcript variant 1, mRNA [NM_032895]	1.02
CYP1A1	Homo sapiens cytochrome P450, family 1, subfamily A, polypeptide 1 (CYP1A1), mRNA [NM_000499]	1.02
LYPD6	Homo sapiens LY6/PLAUR domain containing 6 (LYPD6), mRNA [NM_194317]	1.02
MBNL1	Homo sapiens muscleblind-like (Drosophila) (MBNL1), transcript variant 6, mRNA [NM_207296]	1.02
LOC100133236	PREDICTED: Homo sapiens hypothetical protein LOC100133236 (LOC100133236), mRNA [XM_001714262]	1.02
BNIP3L	Homo sapiens BCL2/adenovirus E1B 19kDa interacting protein 3-like (BNIP3L), mRNA [NM_004331]	1.02
ST7OT1	Homo sapiens ST7 overlapping transcript 1 (non-protein coding) (ST7OT1), non-coding RNA [NR_002330]	1.02
SPANXD	Homo sapiens SPANX family, member D (SPANXD), mRNA [NM_032417]	1.02
FBXO32	Homo sapiens F-box protein 32 (FBXO32), transcript variant 1, mRNA [NM_058229]	1.02
C6orf199	Homo sapiens chromosome 6 open reading frame 199 (C6orf199), mRNA [NM_145025]	1.02
SGMS2	Homo sapiens sphingomyelin synthase 2 (SGMS2), transcript variant 1, mRNA [NM_152621]	1.02
PLAG1	Homo sapiens pleiomorphic adenoma gene 1 (PLAG1), transcript variant 1, mRNA [NM_002655]	1.01
ZNF808	Homo sapiens zinc finger protein 808 (ZNF808), mRNA [NM_001039886]	1.01
HSD17B12	Homo sapiens hydroxysteroid (17-beta) dehydrogenase 12 (HSD17B12), mRNA [NM_016142]	1.01
FOSL1	Homo sapiens FOS-like antigen 1 (FOSL1), mRNA [NM_005438]	1.01
ZNF238	Homo sapiens zinc finger protein 238 (ZNF238), transcript variant 2, mRNA [NM_006352]	1.01
RAB3B	Homo sapiens RAB3B, member RAS oncogene family (RAB3B), mRNA [NM_002867]	1.01
PTX3	Homo sapiens pentraxin-related gene, rapidly induced by IL-1 beta (PTX3), mRNA [NM_002852]	1.00

Table S2 List of the Genes Down-regulated by 100 μg / mL of ZnO-NPs in A549 cells.

Gene symbol	Description	Fold change
KIAA1199	Homo sapiens KIAA1199 (KIAA1199), mRNA [NM_018689]	-2.61
CBLN2	Homo sapiens cerebellin 2 precursor (CBLN2), mRNA [NM_182511]	-1.93
LOC553137	Homo sapiens cDNA FLJ42409 fis, clone BLADE2000866. [AK124400]	-1.86
SLC39A10	Homo sapiens solute carrier family 39 (zinc transporter), member 10 (SLC39A10), transcript variant 2, mRNA [NM_020342]	-1.79
BAAT	Homo sapiens bile acid Coenzyme A: amino acid N-acyltransferase (glycine N-choloyltransferase) (BAAT), transcript variant 1, mRNA [NM_001701]	-1.77
CPLX2	Homo sapiens complexin 2 (CPLX2), transcript variant 1, mRNA [NM_006650]	-1.74
TMEM37	Homo sapiens transmembrane protein 37 (TMEM37), mRNA [NM_183240]	-1.68
HLA-DMB	Homo sapiens major histocompatibility complex, class II, DM beta (HLA-DMB), mRNA [NM_002118]	-1.68
LGALS2	Homo sapiens lectin, galactoside-binding, soluble, 2 (LGALS2), mRNA [NM_006498]	-1.67
GPX2	Homo sapiens glutathione peroxidase 2 (gastrointestinal) (GPX2), mRNA [NM_002083]	-1.65
FGG	Homo sapiens fibrinogen gamma chain (FGG), transcript variant gamma-A, mRNA [NM_000509]	-1.63
DACT2	Homo sapiens dapper, antagonist of beta-catenin, homolog 2 (Xenopus laevis) (DACT2), mRNA [NM__214462]	-1.59
SYT13	Homo sapiens synaptotagmin XIII (SYT13), mRNA [NM_020826]	-1.58
C4orf18	Homo sapiens chromosome 4 open reading frame 18 (C4orf18), transcript variant 2, mRNA [NM_016613]	-1.56
OLFML3	Homo sapiens olfactomedin-like 3 (OLFML3), mRNA [NM_020190]	-1.56
VAV3	Homo sapiens vav 3 guanine nucleotide exchange factor (VAV3), transcript variant 1, mRNA [NM_006113]	-1.54
PRICKLE2	Homo sapiens prickle homolog 2 (Drosophila) (PRICKLE2), mRNA [NM_198859]	-1.54
C12orf27	Homo sapiens chromosome 12 open reading frame 27 (C12orf27), non-coding RNA [NR_024345]	-1.53
PLCXD3	Homo sapiens phosphatidylinositol-specific phosphoiipase C, X domain containing 3 (PLCXD3), mRNA [NM_001005473]	-1.48
PLA2G4A	Homo sapiens phospholipase A2, group IVA (cytosolic, calcium-dependent) (PLA2G4A), mRNA [NM_024420]	-1.46
GRIK2	Homo sapiens glutamate receptor, ionotropic, kainate 2 (GRIK2), transcript variant 2, mRNA [NM_175768]	-1.46
CCL2	Homo sapiens chemokine (C-C motif) ligand 2 (CCL2), mRNA [NM_002982]	-1.44
IFIT1	Homo sapiens interferon-induced protein with tetratricopeptide repeats 1 (IFIT1), transcript variant 2, mRNA [NM_001548]	-1.42
CORO2A	Homo sapiens coronin, actin binding protein, 2A (CORO2A), transcript variant 1, mRNA [NM_003389]	-1.42
ASOR1	Homo sapiens asialoglycoprotein receptor 1 (ASOR1), mRNA [NM_001671]	-1.41
CD24	Homo sapiens CD24 signal transducer mRNA, complete cds and 3' region. [L33930]	-1.38
SFRP4	Homo sapiens secreted frizzled-related protein 4 (SFRP4), mRNA [NM_003014]	-1.38
INSL4	Homo sapiens insulin-like 4 (placenta) (INSL4), mRNA [NM_002195]	-1.36
CLDN2	Homo sapiens claudin 2 (CLDN2), mRNA [NM_020384]	-1.35
SULT2B1	Homo sapiens sulfotransferase family, cytosolic, 2B, member 1 (SULT2B1), transcript variant 1, mRNA [NM_004605]	-1.34
USH1C	Homo sapiens Usher syndrome 1C (autosomal recessive, severe) (USH1C), transcript variant 1, mRNA [NM_005709]	-1.33
CP	Homo sapiens ceruloplasmin (ferroxidase) (CP), mRNA [NM_000096]	-1.32
MUC5AC	Homo sapiens mucin 5AC, oligomeric mucus/gel-forming (MUC5AC), mRNA [NM_017511]	-1.32
CDH1	Homo sapiens cadherin 1, type 1, E-cadherin (epithelial) (CDH1), mRNA [NM_004360]	-1.31
TC2N	Homo sapiens tandem C2 domains, nuclear (TC2N), transcript variant 1, mRNA [NM_152332]	-1.31
PHYHIPL	Homo sapiens phytanoyl-CoA 2-hydroxylase interacting protein-like (PHYHIPL), transcript variant 1, mRNA [NM_032439]	-1.30
NPY1R	Homo sapiens neuropeptide Y receptor Y1 (NPY1R), mRNA [NM_000909]	-1.30
DIRAS3	Homo sapiens DIRAS family, GTP-binding RAS-like 3 (DIRAS3), mRNA [NM_004675]	-1.30
DEFB1	Homo sapiens defensin, beta 1 (DEFB1), mRNA [NM_005218]	-1.29

Gene symbol	Description	Fold change
ELMO1	Homo sapiens engulfment and cell motility 1 (ELMO1), transcript variant 1, mRNA [NM_014800]	-1.29
RNF43	Homo sapiens ring finger protein 43 (RNF43), mRNA [NM_017763]	-1.28
AKR1C3	Homo sapiens aldo-keto reductase family 1, member C3 (3-alpha hydroxysteroid dehydrogenase, type II) (AKR1C3), mRNA [NM_003739]	-1.27
OLFML2A	Homo sapiens olfactomedin-like 2A (OLFML2A), mRNA [NM_182487]	-1.27
BTBD11	Homo sapiens BTB (POZ) domain containing 11 (BTBD11), transcript variant a, mRNA [NM_001018072]	-1.26
A1CF	Homo sapiens APOBEC1 complementation factor (A1CF), transcript variant 3, mRNA [NM_138933]	-1.26
HS3ST3B1	Heparan sulfate glucosamine 3-O-sulfotransferase 3B1 (EC 2.8.2.30)(Heparan sulfate D-glucosaminyl 3-O-sulfotransferase 3B1)(Heparan sulfate 3-O-sulfotransferase 3D1)(h3-OST-3D) [Source:UniProtKB/Swiss-Prot,Acc:Q9Y662] [ENST00000360954]	-1.26
CFH	Homo sapiens complement factor H (CFH), transcript variant 1, mRNA [NM_000186]	-1.25
C5	Homo sapiens complement component 5 (C5), mRNA [NM_001735]	-1.25
SGK493	Homo sapiens protein kinase-like protein SgK493 (SGK493), mRNA [NM_138370]	-1.25
LOC554207	Homo sapiens hypothetical LOC554207, mRNA (cDNA clone MGC:21504 IMAGE:3882600), complete cds. [BC031469]	-1.25
IGSF11	Homo sapiens immunoglobulin superfamily, member 11 (IGSF11), transcript variant 1, mRNA [NM_152358]	-1.24
NOSTRIN	Homo sapiens nitric oxide synthase trafficker (NOSTRIN), transcript variant 1, mRNA [NM_052946]	-1.24
NTRK3	Homo sapiens neurotrophic tyrosine kinase, receptor, type 3 (NTRK3), transcript variant 2, mRNA [NM_002530]	-1.24
NPNT	Homo sapiens nephronectin (NPNT), mRNA [NM_001033047]	-1.23
ADAMTS9	Homo sapiens ADAM metallopeptidase with thrombospondin type 1 motif, 9 (ADAMTS9), mRNA [NM_182920]	-1.23
HHIPL2	Homo sapiens HHIP-like 2 (HHIPL2), mRNA [NM_024746]	-1.23
TM4SF20	Homo sapiens transmembrane 4 L six family member 20 (TM4SF20), mRNA [NM_024795]	-1.21
VIL1	Homo sapiens villin 1 (VIL1), mRNA [NM_007127]	-1.20
RHOV	Homo sapiens ras homolog gene family, member V (RHOV), mRNA [NM_133639]	-1.20
SLC23A1	Homo sapiens solute carrier family 23 (nucleobase transporters), member 1 (SLC23A1), transcript variant 2, mRNA [NM_152685]	-1.20
NR1H4	Homo sapiens nuclear receptor subfamily 1, group H, member 4 (NR1H4), mRNA [NM_005123]	-1.20
NPY5R	Homo sapiens neuropeptide Y receptor Y5 (NPY5R), mRNA [NM_006174]	-1.18
FGB	Homo sapiens fibrinogen beta chain (FGB), mRNA [NM_005141]	-1.17
KCNV1	Homo sapiens potassium channel, subfamily V, member 1 (KCNV1), mRNA [NM_014379]	-1.17
STYK1	Homo sapiens serine/threonine/tyrosine kinase 1 (STYK1), mRNA [NM_018423]	-1.16
FAM171B	Homo sapiens mRNA for KIAA1946 protein. [AB075826]	-1.16
CYP4F3	Homo sapiens mRNA for leukotriene B4 omega-hydroxylase, complete cds. [AB002454]	-1.14
UGT1A6	Homo sapiens UDP glucuronosyltransferase 1 family, polypeptide A6 (UGT1A6), transcript variant 1, mRNA [NM_001072]	-1.14
ST8SIA4	Homo sapiens ST8 alpha-N-acetyl-neuraminide alpha-2,8-sialyltransferase 4 (ST8SIA4), transcript variant 1, mRNA [NM_005668]	-1.13
ATP8B3	Homo sapiens ATPase, class I, type 8B, member 3 (ATP8B3), mRNA [NM_138813]	-1.13
EPCAM	Homo sapiens epithelial cell adhesion molecule (EPCAM), mRNA [NM_002354]	-1.13
ITIH2	Homo sapiens inter-alpha (globulin) inhibitor H2 (ITIH2), mRNA [NM_002216]	-1.13
DKK1	Homo sapiens dickkopf homolog 1 (Xenopus laevis) (DKK1), mRNA [NM_012242]	-1.12
ZNRF3	Homo sapiens zinc and ring finger 3 (ZNRF3), mRNA [NM_032173]	-1.11
hCG_1776007	Homo sapiens hexaribonucleotide binding protein 3 (HRNBP3), mRNA [NM_001082575]	-1.11
MYO10	Homo sapiens myosin X (MYO10), mRNA [NM_012334]	-1.11
CFI	Homo sapiens complement factor I (CFI), mRNA [NM_000204]	-1.10
KIF13A	Homo sapiens kinesin family member 13A (KIF13A), transcript variant 1, mRNA [NM_022113]	-1.10
GPRC5B	Homo sapiens G protein-coupled receptor, family C, group 5, member B (GPRC5B), mRNA [NM_016235]	-1.09
SLC7A7	Homo sapiens solute carrier family 7 (cationic amino acid transporter, y+ system), member 7 (SLC7A7), transcript variant 1, mRNA [NM_003982]	-1.09
FAM83A	Homo sapiens family with sequence similarity 83, member A (FAM83A), transcript variant 2, mRNA [NM_207606]	-1.09
AKR1C1	Homo sapiens aldo-keto reductase family 1, member C1 (dihydrodiol dehydrogenase 1; 20-alpha (3-alpha)-hydroxysteroid dehydrogenase) (AKR1C1), mRNA [NM_001353]	-1.09

Gene symbol	Description	Fold-change
ARHGAP26	Homo sapiens Rho GTPase activating protein 26 (ARHGAP26), transcript variant 1, mRNA [NM_015071]	-1.07
HPGD	Homo sapiens hydroxyprostaglandin dehydrogenase 15-(NAD) (HPGD), mRNA [NM_000860]	-1.07
CPN1	Homo sapiens carboxypeptidase N, polypeptide 1 (CPN1), mRNA [NM_001308]	-1.06
PPARGC1A	Homo sapiens peroxisome proliferator-activated receptor gamma, coactivator 1 alpha (PPARGC1A), mRNA [NM_013261]	-1.06
HLA-DPB1	Homo sapiens major histocompatibility complex, class II, DP beta 1 (HLA-DPB1), mRNA [NM_002121]	-1.06
BCMO1	Homo sapiens beta-carotene 15,15'-monooxygenase 1 (BCMO1), mRNA [NM_017429]	-1.05
PACSIN1	Homo sapiens protein kinase C and casein kinase substrate in neurons 1 (PACSIN1), mRNA [NM_020804]	-1.05
RIPK4	Homo sapiens receptor-interacting serine-threonine kinase 4 (RIPK4), mRNA [NM_020639]	-1.04
CEACAM6	Homo sapiens carcinoembryonic antigen-related cell adhesion molecule 6 (non-specific cross reacting antigen) (CEACAM6), mRNA [NM_002483]	-1.04
FGA	Homo sapiens fibrinogen alpha chain (FGA), transcript variant alpha, mRNA [NM_021871]	-1.04
GPR37	Homo sapiens G protein-coupled receptor 37 (endothelin receptor type B-like) (GPR37), mRNA [NM_005302]	-1.04
SLC23A2	Homo sapiens solute carrier family 23 (nucleobase transporters), member 2 (SLC23A2), transcript variant 2, mRNA [NM_203327]	-1.04
CDH17	Homo sapiens cadherin 17, LI cadherin (liver-intestine) (CDH17), mRNA [NM_004063]	-1.04
UPK1B	Homo sapiens uroplakin 1B (UPK1B), mRNA [NM_006952]	-1.03
SLC22A3	Homo sapiens solute carrier family 22 (extraneuronal monoamine transporter), member 3 (SLC22A3), mRNA [NM_021977]	-1.03
C4BPA	Homo sapiens complement component 4 binding protein, alpha (C4BPA), mRNA [NM_000715]	-1.03
C5orf23	Homo sapiens chromosome 5 open reading frame 23 (C5orf23), mRNA [NM_024563]	-1.03
HGD	Homo sapiens homogentisate 1,2-dioxygenase (homogentisate oxidase) (HGD), mRNA [NM_000187]	-1.03
CCND3	Homo sapiens cyclin D3 (CCND3), transcript variant 2, mRNA [NM_001760]	-1.02

Gene symbol	Description	Fold-change
RAP1GAP	Homo sapiens RAP1 GTPase activating protein (RAP1GAP), mRNA [NM_002885]	-1.02
TBXAS1	Homo sapiens thromboxane A synthase 1 (platelet) (TBXAS1), transcript variant TXS-II, mRNA [NM_030984]	-1.02
CPNE4	Homo sapiens copine IV (CPNE4), mRNA [NM_130808]	-1.01
MAP7	Homo sapiens microtubule-associated protein 7 (MAP7), mRNA [NM_003980]	-1.01
F5	Homo sapiens coagulation factor V (proaccelerin, labile factor) (F5), mRNA [NM_000130]	-1.01
SMC1A	Homo sapiens structural maintenance of chromosomes 1A (SMC1A), mRNA [NM_006306]	-1.01
FGFR3	Homo sapiens fibroblast growth factor receptor 3 (FGFR3), transcript variant 1, mRNA [NM_000142]	-1.01
SYT6	Homo sapiens synaptotagmin VI (SYT6), mRNA [NM_205848]	-1.01
PDZK1	Homo sapiens PDZ domain containing 1 (PDZK1), mRNA [NM_002614]	-1.00
NCALD	Homo sapiens neurocalcin delta (NCALD), transcript variant 7, mRNA [NM_001040630]	-1.00

Table S3 List of the Genes Up-regulated by 20 μg / mL of $ZnCl_2$.

Gene symbol	Description	Fold-change
MT1F*	Homo sapiens metallothionein 1F (MT1F), mRNA [NM_005949]	3.53
CXCL1	Homo sapiens chemokine (C-X-C motif) ligand 1 (melanoma growth stimulating activity, alpha) (CXCL1), mRNA [NM_001511]	1.87
MT2A*	Homo sapiens metallothionein 2A (MT2A), mRNA [NM_005953]	1.54
MT1G*	Homo sapiens metallothionein 1G (MT1G), mRNA [NM_005950]	1.53
C15orf48	Homo sapiens chromosome 15 open reading frame 48 (C15orf48), transcript variant 2, mRNA [NM_032413]	1.46
MT1A*	Homo sapiens metallothionein 1A (MT1A), mRNA [NM_005946]	1.45
ZDHHC21	Homo sapiens zinc finger, DHHC-type containing 21 (ZDHHC21), mRNA [NM_178566]	1.40
ANG	Homo sapiens angiogenin, ribonuclease, RNase A family, 5 (ANG), transcript variant 1, mRNA [NM_001145]	1.35
MT1H*	Homo sapiens metallothionein 1H (MT1H), mRNA [NM_005951]	1.34
CCL5	Homo sapiens chemokine (C-C motif) ligand 5 (CCL5), mRNA [NM_002985]	1.31
STT3B	Homo sapiens STT3, subunit of the oligosaccharyltransferase complex, homolog B (S. cerevisiae) (STT3B), mRNA [NM_178862]	1.31
MT1X*	Homo sapiens metallothionein 1X (MT1X), mRNA [NM_005952]	1.29
DHRS2*	Homo sapiens dehydrogenase/reductase (SDR family) member 2 (DHRS2), transcript variant 1, mRNA [NM_182908]	1.24
SCD	Homo sapiens stearoyl-CoA desaturase (delta-9-desaturase) (SCD), mRNA [NM_005063]	1.22
IL6	Homo sapiens interleukin 6 (interferon, beta 2) (IL6), mRNA [NM_000600]	1.20
GLB1L	Homo sapiens galactosidase, beta 1-like (GLB1L), mRNA [NM_024506]	1.18
JUP	Homo sapiens junction plakoglobin (JUP), transcript variant 1, mRNA [NM_002230]	1.14
ANPEP	Homo sapiens alanyl (membrane) aminopeptidase (ANPEP), mRNA [NM_001150]	1.12
HHIPL2	Homo sapiens HHIP-like 2 (HHIPL2), mRNA [NM_024746]	1.11
C16orf73	Homo sapiens chromosome 16 open reading frame 73 (C16orf73), mRNA [NM_152764]	1.10
MT1B*	Homo sapiens metallothionein 1B (MT1B), mRNA [NM_005947]	1.09

Gene symbol	Description	Fold-change
MAFK	Homo sapiens v-maf musculoaponeurotic fibrosarcoma oncogene homolog K (avian) (MAFK), mRNA [NM_002360]	1.08
NMB	Homo sapiens neuromedin B (NMB), transcript variant 1, mRNA [NM_021077]	1.06
ERAP2	Homo sapiens endoplasmic reticulum aminopeptidase 2 (ERAP2), transcript variant 1, mRNA [NM_022350]	1.05
ULK1	Homo sapiens unc-51-like kinase 1 (C. elegans) (ULK1), mRNA [NM_003565]	1.05
NNMT	Homo sapiens nicotinamide N-methyltransferase (NNMT), mRNA [NM_006169]	1.04
CRYAB	Homo sapiens crystallin, alpha B (CRYAB), mRNA [NM_001885]	1.03
SNX10	Homo sapiens sorting nexin 10 (SNX10), mRNA [NM_013322]	1.02
PDCD4	Homo sapiens programmed cell death 4 (neoplastic transformation inhibitor) (PDCD4), transcript variant 2, mRNA [NM_145341]	1.01

Table S4 List of the Genes Down-regulated by 20 μg / mL of $ZnCl_2$.

Gene symbol	Description	Fold change
TMEM127	Homo sapiens transmembrane protein 27 (TMEM127), mRNA [NM_030665]	-1.66
QKI	Homo sapiens quaking homolog, KH domain RNA binding (mouse) (QKI), transcript variant 1, mRNA [NM_006775]	-1.64
CPM	Homo sapiens carboxypeptidase M (CPM), transcript variant 1, mRNA [NM_001874]	-1.43
BTN2A1	Homo sapiens butyrophilin, subfamily 2, member A1 (BTN2A1), transcript variant 2, mRNA [NM_078476]	-1.38
HSP90AA1	Homo sapiens heat shock protein 90kDa alpha (cytosolic), class A member 1 (HSP90AA1), transcript variant 2, mRNA [NM_005348]	-1.33
UACA	Homo sapiens uveal autoantigen with coiled-coil domains and ankyrin repeats (UACA), transcript variant 2, mRNA [NM_001080821]	-1.32
FAM83D	Homo sapiens family with sequence similarity 83, member D (FAM83D), mRNA [NM_030919]	-1.32
LEPROT	Homo sapiens leptin receptor overlapping transcript (LEPROT), mRNA [NM_017526]	-1.28
CENPA	Homo sapiens centromere protein A (CENPA), transcript variant 1, mRNA [NM_001809]	-1.27
PABPC3	Homo sapiens polyA(A) binding protein, cytoplasmic 3 (PABPC3), mRNA [NM_030979]	-1.22
CAV3	Homo sapiens caveolin 3 (CAV3), transcript variant 1, mRNA [NM_033337]	-1.20
CPA4	Homo sapiens carboxypeptidase A4 (CPA4), mRNA [NM_016352]	-1.19
IRS1	Homo sapiens insulin receptor substrate 1 (IRS1), mRNA [NM_005544]	-1.18
BAT2D1	Homo sapiens BAT2 domain containing 1 (BAT2D1), mRNA [NM_015172]	-1.17
MYLK	Homo sapiens myosin light chain kinase (MYLK), transcript variant 1, mRNA [NM_053025]	-1.15
PL-5283	Homo sapiens PL-5283 protein (PL-5283), mRNA [NM_001130929]	-1.12
KIAA0802	Homo sapiens KIAA0802 (KIAA0802), mRNA [NM_015210]	-1.12
DDX6	Homo sapiens DEAD (Asp-Glu-Ala-Asp) box polypeptide 6 (DDX6), mRNA [NM_004397]	-1.11
C8orf38	Homo sapiens chromosome 8 open reading frame 38 (C8orf38), mRNA [NM_152416]	-1.11
GOSR1	Homo sapiens golgi SNAP receptor complex member 1 (GOSR1), transcript variant 1, mRNA [NM_004871]	-1.10
AK3	Homo sapiens adenylate kinase 3 (AK3), nuclear gene encoding mitochondrial protein, mRNA [NM_016282]	-1.09
ZNF319	Homo sapiens zinc finger protein 319 (ZNF319), mRNA [NM_020807]	-1.08
PDCD5	Homo sapiens programmed cell death 5 (PDCD5), mRNA [NM_004708]	-1.08
KIF20A	Homo sapiens kinesin family member 20A (KIF20A), mRNA [NM_005733]	-1.08
ANXA3	Homo sapiens annexin A3 (ANXA3), mRNA [NM_005139]	-1.08
SIET	Homo sapiens SIET nucleus oncogene (SIET), transcript variant 2, mRNA [NM_003011]	-1.07
SLC27A2	Homo sapiens solute carrier family 27 (fatty acid transporter), member 2 (SLC27A2), mRNA [NM_003645]	-1.06
PTBP1	Homo sapiens polypyrimidine tract binding protein 1 (PTBP1), transcript variant 1, mRNA [NM_002819]	-1.06
UGCG	Homo sapiens UDP-glucose ceramide glucosyltransferase (UGCG), mRNA [NM_003358]	-1.06
SGK493	Homo sapiens protein kinase-like protein Sgk493 (SGK493), mRNA [NM_138370]	-1.05
NFE2L3	Homo sapiens nuclear factor (erythroid-derived 2)-like 3 (NFE2L3), mRNA [NM_004289]	-1.05
TROVE2	Homo sapiens TROVE domain family, member 2 (TROVE2), transcript variant 1, mRNA [NM_001042349]	-1.04
MGC2707	Homo sapiens translation initiation factor eIF-2B, subunit alpha/beta/delta-like protein (MGC27077), transcript variant 1, mRNA [NM_001031727]	-1.04
LMNB2	Homo sapiens lamin B2 (LMNB2), mRNA [NM_032737]	-1.03
PKP2	Homo sapiens phosphoribosyl pyrophosphate synthetase 2 (PRPS2), transcript variant 1, mRNA [NM_001018061]	-1.03
IGFBP7	Homo sapiens insulin-like growth factor binding protein 7 (IGFBP7), mRNA [NM_001553]	-1.03
CCND1	Homo sapiens cyclin D1 (CCND1), mRNA [NM_053056]	-1.00

Journal of
Nanoscience and Nanotechnology
Vol. 13, 161–170, 2013

RESEARCH ARTICLE

Cytotoxic and Genotoxic Effects of Silver Nanoparticles on Primary Syrian Hamster Embryo (SHE) Cells

Xuefei Li[1,2], Liming Xu[1,2,*], Anliang Shao[1], Gang Wu[2,*], and Nobutaka Hanagata[3]

[1] *Institute for Medical Devices Control, National Institutes for Food and Drug Control, No. 2, Temple of Heaven, Beijing 100050, China*
[2] *Baotou Medical College, Inner Mongolia University of Science and Technology, Baotou 014010, China*
[3] *Interdisciplinary Laboratory for Nanoscale Science and Technology, National Institute for Materials Science, 1-2-1 Sengen, Tsukuba, Ibaraki 305-0047, Japan*

Silver-nanoparticles (NPs) have become increasingly common in various applications, raising some safety concerns. In this study, the cytotoxic and genotoxic effects of silver-NPs on primary Syrian hamster embryo (SHE) cells were investigated. Cell viability was assessed using a methyl tetrazolium (MTT) assay, and genotoxic potential was evaluated using a cytokinesis-block micronucleus (CBMN) assay. The results showed that dose-dependent cytotoxicity was induced after 24 h of exposure to silver-NPs. The micronucleation frequency (MNF) also increased significantly in a dose-dependent manner ($P < 0.05$), suggesting that silver-NPs induce genotoxicity. This is consistent with an increased MNF observed in primary SHE cells. The results of cell cycle analysis indicate that the cell cycles became arrested in the *G0/G1* phase and that the *S* phase shortened after only 8 h of silver-NP exposure, suggesting that DNA replication had been inhibited, which in turn inhibited further cell proliferation. The rate of late-stage apoptosis increased after 12 h of silver-NP exposure, and both early- and late-stage apoptosis were obviously increased after 72 h of exposure than in controls. This study demonstrated that silver-NPs could induce strong cytotoxicity and significant genotoxicity in primary SHE cells and that this is probably due to silver-NP-induced apoptosis and the inhibition of cell proliferation.

Keywords: Silver-NPs, Primary Syrian Hamster Embryo (SHE) Cells, Cytotoxicity, Genotoxicity, Cell Cycles, Apoptosis.

1. INTRODUCTION

Nanomaterials are seeing increasingly frequent use in commercial applications because of their novel physicochemical properties. However, concerns have arisen regarding the adverse effects of nanomaterials on human health and the environment.[1] Nanomaterials have been shown to induce toxicity in cells, tissues, and organs.[2–7] Of the various nanomaterials, silver-nanoparticles (NPs) are the most commonly used in consumer and industrial products, including medical products and devices, food storage materials, and various health care products. This is largely due to their antibacterial activity.[8–12] Consequently, silver-NPs have also raised the most safety concerns. Silver-NP-induced cytotoxicity and genotoxicity have been observed in many *in vivo* and *in vitro* studies.[13–23]

Many of these studies have suggested that silver-NP treatment can increase DNA damage and chromosome aberrations in various types of cells.[19,21,22,24] However, most of these studies have been based on particular cell lines. One study showed that chromosomal aberrations occurred in 20% of U251 human glioblastoma cells subjected to silver-NP treatment, but also occurred in 16% of untreated cells.[21] In contrast, silver-NP-treated IMR-90 cells, which are normal human lung fibroblasts, showed an aberration rate of 10%, and untreated control cells showed no chromosome aberrations.[21] These findings show that cancer cells have a higher rate of spontaneous chromosome aberration, suggesting that these cells are not suitable for genotoxicity testing; but normal cells have a lower rate of spontaneous chromasone aberration, making these cells are suitable for genotoxicity testing. In the present study, primary Syrian hamster embryo (SHE) cells were used to determine the genotoxic potential of silver-NPs.

*Authors to whom correspondence should be addressed.

Reactive oxygen species (ROS) induce oxidative damage in DNA. In this way, they play an important role in the cytotoxicity and genotoxicity of nanomaterials.[7,25–28] The cytokinesis-block micronucleus (CBMN) assay is based on the blocking of cytokinesis by cytochalasin B (Cyt-B), which can express micronuclei produced in response to chromosome breakage or damage to the mitotic apparatus.[29–31] In the present study, a CBMN assay was chosen to assess the genotoxic potential of silver nanoparticles on primary SHE cells.

2. MATERIALS AND METHODS

2.1. Test Materials and Characterization

Silver-NPs (size ≤ 100 nm, approx. 99.5%) were purchased from Sigma-Aldrich (St. Louis, MO, U.S.). Silver-NP was dissolved in distilled water and cell culture media and dispersed using ultrasonication for 10 min. The size distribution was determined using dynamic light scattering (DLS). Drops of silver particle solution were placed on a copper net for observation of size morphology using transmission electronic microscopy (TEM). The zeta potentials (ZPs) associated with the silver nanoparticles were also determined to assess their stability in solution and possible interactions with the media using a Malvern Zeta Sizer Nano ZS (Malvern Instruments, Worcestershire, U.K.) operating with Dispersion Technology Software version 5.03 (DTS Nano).

2.2. Chemicals

Thiazolyl blue tetrazolium bromide, 3-(4, 5-dimethylthyl-thiazol-2, 5- diphenyltetrazolium bromide (MTT, ≥ 97.5%), cytochalasin B (Cyt-B), and mitomycin C (MMC) were used. The MTT was dissolved in phosphate-buffered saline (PBS, 5 mg/mL), the Cyt-B was dissolved in dimethyl sulfoxide (DMSO, 2.0 mg/mL), and the MMC was dissolved in NaCl solution (10 μg/mL) for use as stock solution. All solutions were sterilized before use by filtration through a 0.2 μm-pore film and stored at −20 °C.

2.3. Animals

Syrian golden hamsters at day 13 of gestation were purchased from Beijing Wei Tong Li Hua Experimental Animal Technology Co., Ltd. (Beijing, China). Animal experiments were conducted in compliance with China's national ethical standards.

2.4. Solutions and Reagents

Wash solution for cell isolation: calcium-magnesium-free Hanks Balanced Salt Solution (CMF-HBSS, Gibco, U.S.) containing 200 U/mL of penicillin and 200 μg/mL of streptomycin (Gibco, U.S.); dissociation solution (prepared on the day of cell isolation): CMF-HBSS containing 1.25% (v/v) of trypsin and 2.5% (v/v) of pancreatin (Sigma, U.S.), 200 U/mL of penicillin, and 200 μg/mL of streptomycin (solution pH was adjusted to 7.0–7.2 before use by adding 7.5% sodium bicarbonate solution); cell isolation media and complete culture media: 500 mL of Dulbecco's Modified Eagle high-glucose medium (DMEM, Gibco, U.S.) containing 130 mL of fetal bovine serum (FBS) (Gibco, U.S.), 13 mL of 200 μM L-glutamine (Gibco, U.S.), and 6.5 mL of 10,000 U penicillin and 10,000 μg/mL streptomycin; cryopreservation media: 85 mL of complete culture media, 15 mL of DMSO (Sigma, U.S.); detachment solution: HBSS containing 0.05% trypsin and 0.53 mM EDTA (Sigma, U.S.).

2.5. Cell Isolation and Culture

Embryo cells were isolated from the embryos of two pregnant hamsters on day 13 of gestation. The hamsters were killed via CO_2 asphyxiation, and the uterine horns were removed and transferred to a 50 mL sterile tube containing ice-cold wash solution. The embryos were removed from the horns and transferred to new Petri dishes containing ice-cold wash solution in a class II biosafety cabinet. About 25 embryos (from two pregnant hamsters) were decapitated, eviscerated, and delimbed, and the remaining tissues were placed in a sterile 100 mL beaker containing 10 mL of wash solution. The tissues were minced into smaller (3 mm) pieces using scissors and then rinsed with 80 mL of wash solution by placing the beaker on a stir plate at low speed for 5 min. Once the tissues had settled, the wash solution was discarded. This rinse step was repeated using dissociation solution (room temperature). Then 50 mL of dissociation solution was added to the flask and slowly stirred for 8 min. The cells were collected, and then 2 mL of cold FBS was added to four 50 mL sterile tubes (on ice). The tissues were allowed to settle and the supernatant (containing dissociated cells) were carefully transferred into the prepared tubes. Then 50 mL of fresh dissociation solution was added to the tissues and stirred for 7 min. The cells were then collected as described above. This dissociation step was performed a total of four times. Cells were collected by centrifugation at 1000 rpm for 5 min and then pooled in 40 mL complete culture media containing antibiotics. The cells were filtered using a 70 μm pore filter (BD, U.S.) and left on-ice until seeding. The viable cells were counted using the trypan blue exclusion method and then seeded (1×10^7 viable cells/T-75 flask) with a complete culture medium containing antibiotics. After incubation at 37 °C and 7% CO_2 for 4 h, the culture media were then replaced with 20 mL of complete culture media without antibiotics. After incubation for another 24 h, cell growth reached about 70% confluence. The culture media were then discarded, and the cells were rinsed twice with 10 mL of CMF-HBSS. Then 1 mL of detachment solution was added to each flask and allowed to incubate for 2–3 min. Then 10–20 mL of cold complete culture media without antibiotics was added to stop trypsin activity. The cells were pooled in 40–50 mL of fresh complete culture media without antibiotics. The cells were counted and resuspended in cryopreservation media, which were diluted with culture media (final: 7.5% DMSO) to 2.5×10^6 cells/mL. One milliliter of cell suspension was dispensed into cryostorage vials (Nunc), and the cells were frozen in a −70 °C freezer for 24 h, prior to transfer to and storage under liquid nitrogen.

The cells were cultured in DMEM supplemented with 20% FBS, 4 mM glutamine, 100 U/mL penicillin, and 100 μg/mL streptomycin. The cultures were maintained in a humidified atmosphere at 37 °C with 7% CO_2.

2.6. MTT Assay

The cytotoxicity of the silver-NPs was assessed using the MTT assay by measuring the optical density of the formazan product. Briefly, 1×10^4 SHE cells (at the fourth passage) were seeded into each well of a 96-well plate and cultured for 24 h, reaching 70% cell confluence. The cells were then exposed to silver-NPs at 0, 2.5, 5, 10, 20, and 40 μg/mL for another 24 h. Before being added to the cells, the silver-NPs were diluted in culture media and ultrasonically treated (ultrasonicator; Beijing Jinxing, China) at 300 W, for 10 min. Each dose group was set for 8-repeats. After exposure, the cells were washed, and mixture of 20 μL of MTT (5 mg/mL) and 100 μL of non-phenol-red media was added to the cells and incubated for 4 h. The MTT solution was then discarded, and the cells were washed with PBS. Next, 150 μL of DMSO was added to the cells, and the plate was shaken for 10 min. Then, 100 μL of supernatant from each sample was transferred using a multichannel pipette to a new 96-well plate for assay. This transfer decreased the disturbance caused by the remaining silver-NPs to the optical density (OD) detection. The assay was performed using a plate reader at a wavelength of 570 nm, with 630 nm as the reference wavelength. These results are expressed as cell viability relative to untreated control cells.

The modified Karber formulation $\lg IC_{50} = Xm - I(P - (3 - Pm - Pn)/4)$ was used to estimate the 50% inhibitory concentration (IC_{50}) of silver-NPs to SHE cell viability. The following abbreviations were used: Xm, lg max dose; I, lg (max dose/next dose); P, average inhibition rate; Pm, maximum inhibition rate; Pn, minimum inhibition rate.

2.7. CBMN Assay

A CBMN assay was performed using the protocol described below. The primary SHE cells (fourth passage) were seeded at 5×10^5 cells/35 cm in a cell culture dish and let the cells were allowed to grow to 70–80% confluence for 24 h. Then the cells were exposed to 10, 20, and 40 μg/mL of silver-NPs. The silver-NPs were diluted in culture media before being added to the cells. Then they were ultrasonicated for dispersal (ultrasonicator; Beijing Jinxing, China) at 300 W, for 10 min. MMC (0.1 μg/mL) was used as a positive control, and NaCl (50 μL/mL) was used as a negative control. The cells were then cultured for another 24 h. The cells were washed and then cytochalasin-B (final: 3 μg/mL) was added. The cells were cultured for another 18 h. The cells were collected, and the supernatant was discarded. The cells were hypotonically treated with 2 mL of 0.075 M KCl and allowed to sit at room temperature for 5 min. Then 5 mL of fixing solution (methyl alcohol:acetic acid = 3:1) was added, and the mixture was centrifuged immediately (1000 rpm for 5 min). The supernatant was then discarded, and 5 mL of fresh fixing solution was added. The cells were fixed for over 30 min. The fixing solution was then changed again, and the cells were fixed for another 10 min. Cells were dropped onto the center of a slide. The slides were dried at room temperature and stained using 4% Giemsa solution (pH 6.8) for 30 min.

The slides were scored by two experts blinded to the purpose of the experiment at 400× magnification. The micronucleation frequency (MNF, %) was determined for 1000 binucleated cells (BNCs) per culture, and three cultures were established per group.

2.8. Analysis of the Cell Cycle and Apoptosis

The duration of exposure to silver-NPs (4, 8, 12, 24, and 48 h) was established on the basis of the cell cycles of SHE cells. In brief, 8×10^5 cells were seeded in a 60 cm cell culture dish and allowed to grow to 70% confluence for 24 h. Then, 20 μg/mL silver-NP solution was added to the culture media, and, after ultrasonic treatment, the media were added to the cells. The cells were harvested after the specified lengths of time. The cells were with PBS and fixed in 75% ice-cold alcohol and stored overnight in a freezer at −20 °C. Then the cells were collected, washed again with PBS, and stained using propidium iodide solution (containing RNase, MultiSciences Biotech Co., Ltd., China) for 30 min, protected from light. The samples were analyzed using a flow cytometer (BD FACSCalibur, Becton Dickson, U.S.). For analysis of apoptosis, 10 μL of Annexin V-FITC (BIOSEA Co., Ltd., China) was added to a 200 μL solution containing fresh cells (1×10^6 cells/mL), protected from light. After 15 min, 300 μL of binding buffer and 5 μL of *PI* solution were added. The cell samples were then immediately analyzed using a flow cytometer.

2.9. Statistical Analysis

The data are presented as the mean ± SD. All experiments were repeated at least three times. The data were statistically analyzed using *t*-testing, ANOVA, and Dunnett testing (2-sided) using SPSS version 12. Differences were considered significant at $P < 0.05$.

3. RESULTS

3.1. Characterization of Silver NPs

The morphology of silver-NP in distilled water and in culture medium was observed using TEM (Figs. 1(a) and (b)). Particle size distribution in distilled water, as determined by DLS, was found to be 9.6% 6.3–20 nm; 33.6% 27.3–51 nm; 27.5% 52–106.2 nm; 29.3% 106.2–629.0 nm (Fig. 1(c)). The particle size distribution in cell culture medium was found to be 4.4% 10.1–59.8 nm;

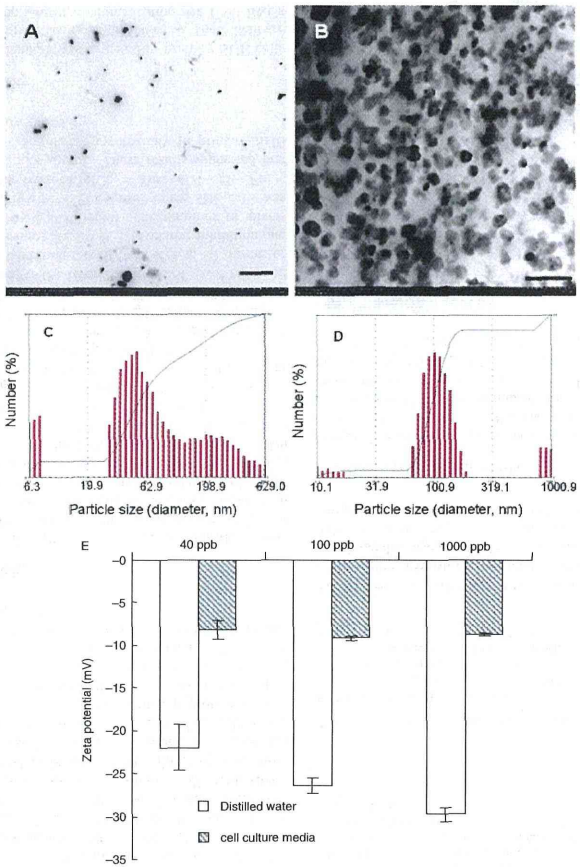

Fig. 1. Characterization of silver-NPs. (a) TEM image of silver-NPs in distilled water (Bar: 1000 nm). (b) Culture media (Bar: 500 nm). (c) Particle size distribution plot of silver-NPs measured by DLS in distilled water. (d) Culture media. (e) Zeta potential of silver-NPs in distilled water and in culture media.

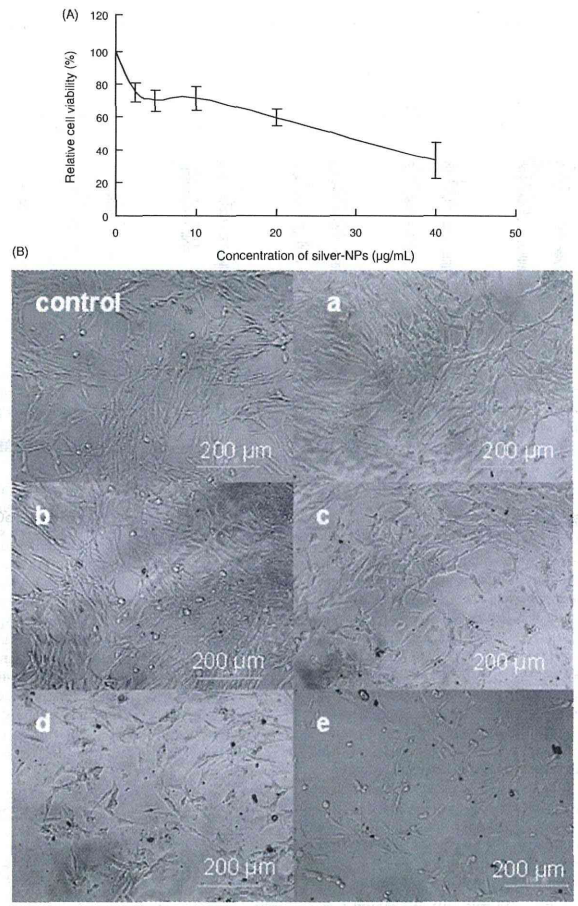

Fig. 2. (a) Relative viability and (b) morphological changes in SHE cells after exposure to different doses of silver-NPs. A relative viability curve was generated from MTT assay. The morphological changes of the cells were observed using light microscopy. Control: untreated cells; (a)–(e): cells exposed to silver-NPs (2.5, 5, 10, 20, and 40 μg/mL), respectively. Magnification: $\times$ 200.

45.7% 59.9–100.9 nm; 40.9% 100.1–189.1 nm; 9% 818.4–1009.0 nm (Fig. 1(d)). The variations in size may be attributable to changes in the hydrodynamic radii of the particles in the different media, which may in turn be due to particle and media interactions. The larger particles (over 100 nm in diameter) were observed in both distilled water and cell culture media (Figs. 1(c) and (d)). This may be due to particle agglomeration upon dispersal in the

media. DLS may indicate the hydrodynamic radius rather than particle size.

The average zeta potential, as measured at silver-NP concentrations of 40, 100, and 1000 ppb were found to be −22.0, −26.4, and −29.8 mV in water and −8.2, −9.2, and −8.76 mV in cell culture media (Fig. 1(e)). Zeta potential values of this nature suggest that, upon dispersion, the particles form an unstable dispersal pattern. The average zeta potentials in cell culture media with silver-NPs were found to be dramatically different from those of silver-NP dissolved in distilled water, suggesting that silver-NPs interact with the components of the cell culture media. This in turn suggests significant protein adsorption by the nanoparticles in the cell growth media. Protein adsorption from the medium is also reflected in the size distribution of the particles, as determined by DLS. This may have an effect on the cellular response to the presence of silver nanoparticles.

3.2. Cytotoxicity

A relative viability curve was generated from MTT assay (Fig. 2(a)). The 50% inhibition concentration (IC_{50}) of silver-NPs exposed to SHE cells for 24 h was estimated on the basis of the MTT assay results. The relative cell viability decreased as the concentration of silver-NPs increased (Fig. 2(a)). Relative inhibition rate of SHE cells which were exposed to silver-NPs at 0, 2.5, 5, 10, 20, and 40 μg/mL were 0, 24.87, 30.37, 28.69, 40.40 and 66.63%, respectively. The cells exposed to the 2.5 μg/mL of silver-NPs had a relative inhibition rate of over 20%, but no significant morphological changes. When the cells exposed to the 5 μg/mL of silver-NPs had a relative inhibition rate of about 30% and some of the cells appeared to have shrunk (Fig. 2(b)). The growth was significantly inhibited when the cells exposed to the 10 or 20 μg/mL of silver-NPs, and had a relative inhibition rate of over 40% at 20 μg/mL of silver-NPs exposure (Fig. 2(b)). The relative inhibition rate was then estimated at different concentrations of silver-NPs. The IC_{50} of silver-NPs exposed to the SHE cells was estimated on the basis of $\lg IC_{50} = Xm - I(P - (3 - Pm - Pn)/4)$ to be 15.24 μg/mL. These results suggested that silver-NPs have significant cytotoxicity to primary SHE cells, even at low doses.

3.3. Genotoxicity

Chromosome damage was detected in primary SHE cells exposed to silver-NP using a CBMN assay. These data are expressed as the rate of micronucleation per 1000 BNCs per culture. Cells treated with MMC (positive control) showed an MNF of 7.67% (Table I, Fig. 3). Cells treated with NaCl (negative control) showed an MNF of 1.6%, and the difference was found to be significant ($P < 0.05$). There was a significant increase ($P < 0.05$) in the frequency of MN for all cells exposed to silver-NPs (Table I, Fig. 3).

Table I. Micronucleation frequency (MNF (%)) of SHE cells treated with MMC (positive control), NaCl (negative control), and silver-NP. The micronucleation frequency was determined for 1000 binucleated cells (BNCs) per culture and in a total 3000 BNCs per concentration. The significance of the difference between the positive control and the negative control was determined using *t*-testing; and the significance of all test samples relative to the negative control was identified using one-way ANOVA and Dunnett tests (2-sided). *, $P < 0.05$. The data represent the mean ± SD ($n = 3$).

Test	Dose	FMN (%)	*P*-value	95% confidence interval of the mean	
				Lower bound	Upper bound
NaCl (sol.)	50 μL/mL	1.6±0.66		−0.029	3.229
	10 μg/mL	2.9±0.66*	0.032	1.27	4.53
Silver-NPs	20 μg/mL	4.03±0.29*	0.001	3.32	4.75
	40 μg/mL	4.83±0.25*	0.0001	4.21	5.46
MMC	0.1 μg/mL	7.67±0.72*	0.0001		

The increase in MNF was not found to be dose-dependent at 40 μg/mL exposure. This may be due to the increases in cell death caused by the high concentration of toxic particles. These results suggested that silver-NPs may induce chromosome damage in primary SHE cells.

3.4. Cell Cycle and Apoptosis

Cell cycle analysis was performed after exposing the SHE cells to 20 μg/mL silver-NPs. The cell cycle and proliferation index (PI) were estimated from the ratio of the S phase, the $G2/M$ phase, and the whole cell cycle using the following formula: $PI = (S + G2/M)/(G0/G1 + S + G2/M)$ at a cell proliferation rate of $PI \times 100\%$ (Table II).

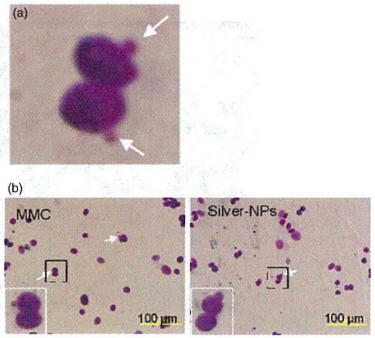

Fig. 3. Giemsa staining of SHE cells treated with MMC (positive control) and silver-NPs. Arrows indicate micronuclei in binucleated cells. (a) Typical micronucleus image in binucleated cell (MMC treatment culture). (b) Positive control (MMC) and silver-NP treatment. Images near the bottom of photo B are magnified micronuclei. Magnification: ×400.

Table II. Cell cycle and proliferation index (PI) of SHE cells exposed to silver-NPs at 20 μg/mL.

Groups	Time (h)	$G0/G1$ (%)	$G2/M$ (%)	S (%)	PI (%)*
Control	4	44.82	43.32	11.86	56.41
	8	47.42	43.05	9.53	53.68
	12	49.51	43.36	7.14	51.51
	24	50.11	39.66	10.24	50.89
	48	68.02	27.90	4.08	32.44
Silver-NPs	4	46.33	41.39	12.28	54.83
	8	64.44	21.54	14.03	36.11
	12	56.03	38.84	5.14	44.76
	24	56.50	32.40	11.11	44.28
	48	76.25	18.82	4.94	24.07

Notes: *PI represents the ratio between the S phase, the $G2/M$phase, and the whole cell cycle. $PI = (S + G2/M)/(G0/G1 + S + G2/M)$; cell proliferation rate = $PI \times 100\%$.

The $G0/G1$ phase was found to be dominant after 8 h exposure, and the S phase was found to be significantly shorter than in untreated control cells, indicating that silver-NPs can arrest the cell cycle during the $G0/G1$ phase in primary SHE cells, and inhibit DNA replication and cell proliferation. The number of cells in the $G2/M$ phase was not found to be significantly different in cells exposed to silver-NPs and in control cells (Fig. 4).

The rate of late-stage apoptosis was lightly increased in the experimental groups than that in the control groups after 12 h exposure, and both early- and late-stage apoptosis were obviously increased after 72 h exposure (Fig. 5(A)–(B2)). These results suggested that apoptosis may play a role in cytotoxicity and genotoxicity of silver-NPs in primary SHE cells.

4. DISCUSSION

One previous study showed that silver-NP treatment can arrest the cell cycle in the $G(2)/M$ phase in U251 cells. This may be due to repair of damaged DNA.[21] In the present study, silver-NP exposure induced cell cycle arrest in the $G0/G1$ phase and significantly shortened the S phase after 8 h of exposure in primary SHE cells, indicating that DNA synthesis, not DNA repair, had been inhibited, and that this was what had inhibited cell proliferation. This cell cycle arrest resolved after 12 h exposure, and the cell cycle arrested in the $G0/G1$ phase was found again at 24 h and 48 h of exposure. This may indicate some cellular response to silver-NP exposure. It is also possible is that the cells had reached full confluence (data not shown) at 24 h or 48 h culture, and this may have caused the cells to cease proliferation. This conclusion is supported by the proliferation index (PI) which was very low in cells exposed to silver-NP exposure, as well as that in the control cells at 24 h and 48 h (Table II).

In this study, the rate of early-stage and late-stage apoptosis of SHE cells exposed to 20 μg/mL of silver-NPs were 6.64% and 8.21%, respectively, which obviously higher than the 3.97% and 4.93% observed in controls. Many studies have suggested that silver-NPs first affect the mitochondria and then basic cellular metabolism. Silver-NPs generate reactive oxygen species upon entering the cells, causing oxidative stress and mitochondrial toxicity.[32] In this study, MTT results, which indicate mitochondrial toxicity, show that the apoptosis induced by silver-NPs in SHE cells was mitochondrially mediated. The cytotoxicity of the silver-NPs, and their ability to induce apoptosis, is affected by particle size, morphology, surface modifications, charge, dispersion, agglomeration, and the type of cell exposed.[32–34] Some investigations have suggested that certain cancer cell lines might be more sensitive to silver-NP toxicity than normal cells and non-cancerous cell lines.[21,32] Mukherjee et al. found HeLa cells to be more sensitive than the HaCaT cells in *in vitro* assays.[32] HeLa cells are a cervical epithelial adenocarcinoma cell line, and HaCaT cells are an immortal non-cancerous human keratinocyte cell line. Mukherjee et al. believed that the

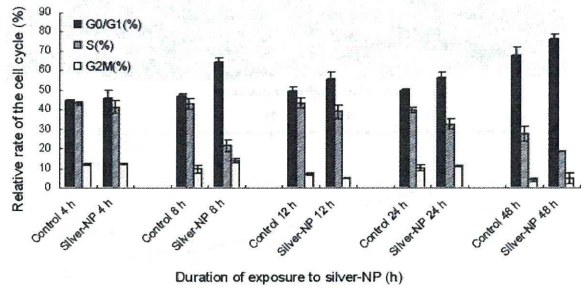

Fig. 4. Cell cycle analysis of SHE cells exposed to silver-NPs for different lengths of time. Data shown are the mean ± SD of three separate experiments. The counted cells containing the complete cell cycle ($G0/G1$, S, and $G2/M$) were taken to represent 100%.

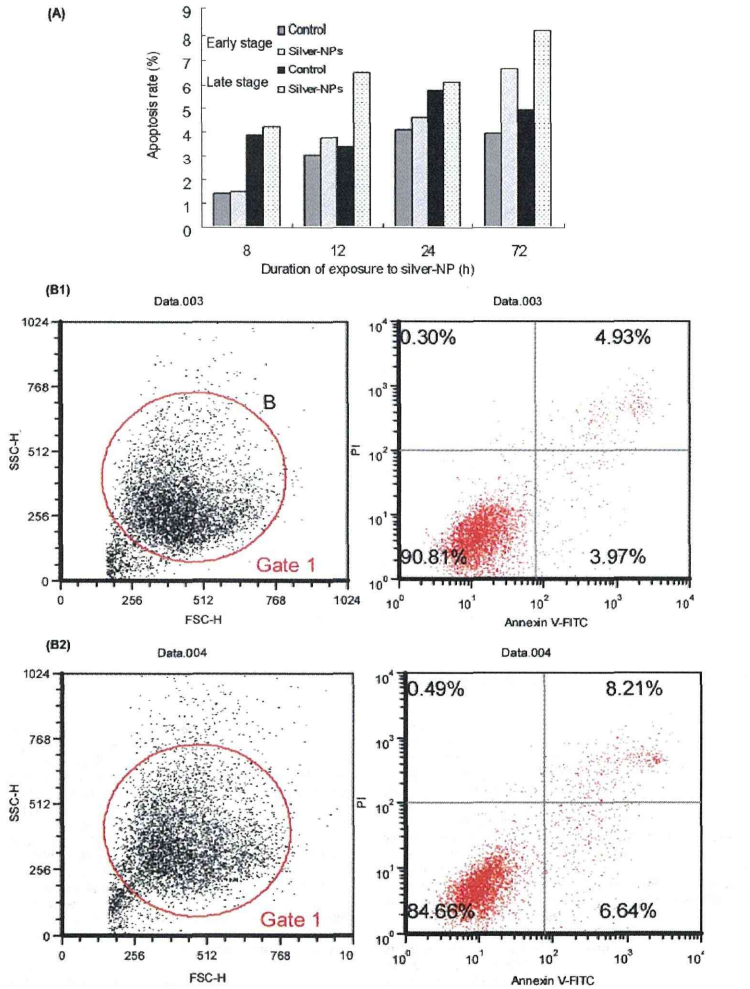

Fig. 5. (A) Rate of late- and early-stage apoptosis (%) among SHE cells in the control group and silver-NP groups (20 μg/mL). Data indicate the relative number of cells the in the gate. The total number of countable was taken as 100% level. Each silver-NP treatment group was compared to a control group that had been exposed to control substances for the same amount of time. The plots obtained using flow cytometric analysis indicated (B1) apoptosis in control cells and (B2) in cells exposed to silver-NP for 72 hours.

difference in the sensitivity of HaCaT and HeLa cells can be understood in terms of the difference in their natural antioxidant levels. In the present study, analysis of apoptosis did not involve comparisons to cancerous cells, but we believe that the normal cells are more suitable to assess toxicity, and more indicative of human cells *in vivo*.

CBMN assays are based on the blocking of cytokinesis by cytochalasin B (Cyt-B). In this way, chromosome damage events are detected only in dividing cells, which, unlike non-dividing cells, are can express the micronuclei produced in response to chromosome breakage or damage to the mitotic apparatus damage.[29–31] Cyt-B eliminates the confounding effect of altered cell division kinetics on micronuclear expression.[30] CBMN assays have been successfully applied to normal human lymphocytes, mouse spleen lymphocytes, mouse fibroblasts, and Chinese hamster lung fibroblasts.[30] In one previous study, a CBMN assay was successfully used on a human B lymphoblastoid cell line, and a significant increase in the frequency of micronucleated binucleation cells was observed when the cells were exposed to hydrogen peroxide or hypoxanthine (HX)/xanthine oxidase (XO), which generates superoxides.[31] In this way, CBMN assays are very sensitive to ROS-mediated DNA damage, making it very suitable for assessment of the nanomaterial-induced genotoxicity. In this study, a CBMN assay showed that silver-NPs at concentrations of 10, 20, and 40 μg/mL of silver-NPs (50.1% < 100 nm in size; 40.9% 100–200 nm; and 9% 818.4–1009.0 nm, as determined by DLS) induced significant increases in MNF in primary SHE cells ($P < 0.05$). Control cells showed a low MNF (1.6%). AshaRani and Hande et al. reported that exposure to 25 μg/ml silver-NPs (6–20 nm in size) induced chromosomal aberrations in 10% of normal IMR-90 cells (and in 0% of control cells) and in 20% of U251 cancer cells (and in 16% of control cells).[21] Kawata et al. showed that exposure to 1.0 μg/ml silver-NPs (7–10 nm in size) induced micronucleus formation in up to 47.9% of exposed HepG2 cells.[19] Hackenberg et al. reported that both a comet assay and chromosomal aberration test indicated DNA damage after 1, 3, and 24 h of exposure to 0.1 μg/mL silver nanoparticles in human mesenchymal stem cells.[35] These findings suggest that sensitivity to silver-NPs differs among cell types. It is likely that cancer cell lines may be more sensitive to genotoxicity than non-cancer cells and may have higher transformation backgrounds. Normal cells may more accurately reflect the exact genotoxicity of the test articles, as indicated in the present study, in which the transformation background of untreated SHE cells was very low (1.6%), as in IMR-90 cells (0%).[22]

To determine the genotoxic and carcinogenic risk of silver-NP in human cells, *in vivo* genotoxicity and carcinogenicity assessment is necessary. In one of our recent studies, vaginal exposure to silver-NP/Gel induced the formation of micronuclei, nuclear disruption, chromatin concentration, and apoptosis in rabbit reproductive organ tissues.[36] In the current study, the potential genotoxic and carcinogenic risk of nanomaterials was assessed on a case-by-case basis. Several studies have provided evidence of nano-specific genotoxicity and tumorigenicity, but other studies have not. This may be due to insufficient characterization of the test material, differences in experimental design, the use of different animal models and species, or differences in dosimetry and target organs.[3] As shown in Japan, it has taken about 10 years until finding that exposure to asbestos nanofibers can have serious carcinogenic effects.[37] Considering the rapid increase in the production and use of silver nanoparticles, it is imperative to gain a thorough understanding of their genotoxicity and carcinogenicity to prevent the human health catastrophe that resulted from widespread use of asbestos fibers.[37]

Acknowledgments: This study was financially supported by the Beijing Natural Science Foundation of China (No. 3112024); the Open Research Fund of State Key Laboratory of Bioelectronics, Southeast University, China (E04); National Key Technology Research and Development Program of the Ministry of Science and Technology of China (2012BAK26B00).

References and Notes

1. J. Zhao and V. J. Castranova, *Toxicol. Environ. Health Part B* 14, 593 (**2011**).
2. M. Ahamed, M. S. AlSalhi, and M. K. J. Siddiqui, *Clin. Chim. Acta* 411, 1841 (**2010**).
3. H. Becker, F. Herzberg, A. Schulte, and M. Kolossa-Gehring, *Int. J. Hyg. Environ. Health* 214, 231 (**2011**).
4. H. Tsuda, J. Xu, Y. Sakai, M. Futakuchi, and K. Fukamachi, *Asian Pac. J. Cancer Prev.* 10, 975 (**2009**).
5. T. M. Tolaymat, A. M. El Badawy, A. Genaidy, K. G. Scheckel, T. P. Luxton, and M. Suidan, *Sci. Total Environ.* 408, 999 (**2010**).
6. L. V. Stebounova, A. Adamcakova-Dodd, J. S. Kim, H. Park, P. T. O'Shaughnessy, V. Grassian and P. S. Thorne, *Part Fibre Toxicol.* 8, 5 (**2011**).
7. M. J. Piao, K. A. Kang, I. Lee, H. S. Kim, S. Kim, J. Y. Choi, J. Choi, and J. W. Hyun, *Toxicol. Lett.* 201, 92 (**2011**).
8. X. Chen and H. J. Schluesener, *Toxicol Lett.* 176, 1 (**2008**).
9. H. H. Lara, E. N. Garza-Treviño, L. Ixtepan-Turrent, and D. K. Singh, *J. Nanobiotechnology* 9, 30 (**2011**).
10. W. J. Yang, C. C. Shen, Q. H. An, J. J. Wang, Q. D. Liu, and Z. Z. Zhang, *Nanotechnology* 20, 085102 (**2009**).
11. G. A. Sotiriou and S. E. Pratsinis, *Environ. Sci. Technol.* 44, 5649 (**2010**).
12. K. Chaloupka, Y. Malam, and A. M. Seifalian, *Trends Biotechnol.* 28, 580 (**2010**).
13. L. Xu, T. Takemura, M. Xu, and N. Hanagata, *Materials Express* 1, 74 (**2011**).
14. L. Xu, X. Li, T. Takemura, N. Hanagata, G. Wu, and L. L. Chou, *J. Nanobiotechnology* 10, 16 (**2012**).
15. Y. S. Kim, M. Y. Song, J. D. Park, K. S. Song, H. R. Ryu, Y. H. Chung, H. K. Chang, J. H. Lee, K. H. Oh, B. J. Kelman, I. K. Hwang, and I. J. Yu, *Part. Fibre. Toxicol.* 7, 20 (**2010**).
16. J. Tang, L. Xiong, G. Zhou, S. Wang, J. Wang, L. Liu, J. Li, F. Yuan, and T. Xi, *J. Nanosci. Nanotechnol.* 9, 4924 (**2009**).

17. J. Tang, L. Xiong, G. Zhou, S. Wang, J. Wang, L. Liu, J. Li, F. Yuan, S. Lu, Z. Wan, L. Chou, and T. Xi, *J. Nanosci. Nanotechnol.* 10, 6313 (**2010**).
18. J. S. Kim, J. H. Sung, J. H. Ji, K. S. Song, J. H. Lee, C. S. Kang, and I. J. Yu, *Saf. Health Work* 2, 34 (**2011**).
19. K. Kawata, M. Osawa, and S. Okabe, *Environ. Sci. Technol.* 43, 6046 (**2009**).
20. N. A. Flower, B. Brabu, M. Revathy, C. Gopalakrishnan, S. V. Raja, S. S. Murugan, and T. S. Kumaravel, *Mutat. Res.* 742, 61 (**2012**).
21. P. V. AshaRani, M. P. Hande, and S. Valiyaveettil, *BMC Cell Biology* 10, 65 (**2009**).
22. P. V. AshaRani, M. Low Kah Mun, M. P. Hande, and S. Valiyaveettil, *ACS Nano.* 3, 279 (**2009**).
23. J. H. Sung, J. H. Ji, K. S. Song, J. H. Lee, K. H. Choi, S. H. Lee, and I. J. YU, *Toxicol. Ind. Health* 27, 149 (**2011**).
24. R. Foldbjerg, D. A. Dang, and H. Autrup, *Arch. Toxicol.* 85, 743 (**2011**).
25. C. Carlson, S. M. Hussain, A. M. Schrand, L. K. Braydich-Stolle, K. L. Hess, R. L. Jones, and J. J. Schlager, *J. Phys. Chem.* 112, 13608 (**2008**).
26. Y. H. Hsin, C. F. Chen, S. Huang, T. S. Shih, P. S. Lai, and P. J. Chueh, *Toxicol. Lett.* 197, 130 (**2008**).
27. M. Valko, C. J. Rhodes, J. Moncol, M. Izakovic, and M. Mazur, *Chem. Biol. Interact.* 160, 1 (**2006**).
28. M. F. Rahman, J. Wang, T. A. Patterson, U. T. Saini, B. L. Robinson, G. D. Newport, R. C. Murdock, J. J. Schlager, S. M. Hussain, and S. F. Ali, *Toxicol. Lett.* 187, 15 (**2009**).
29. M. Fenech, *Environ. Health Perspect.* 101, 101 (**1993**).
30. M. Fenech, *Mutat. Res.* 392, 11 (**1997**).
31. M. Fenech, *Mutat. Res.* 455, 81 (**2000**).
32. S. G. Mukherjee, N. O'Claonadh, A. Casey, and G. Chambers. *Toxicology In Vitro* 26, 238 (**2012**).
33. A. M. El Badawy, R. G. Silva, B. Morris, K. G. Scheckel, M. T. Suidan, and T. M. Tolaymat. *Environ. Sci. Technol.* 45, 283 (**2011**).
34. P. W. Li, T. H. Kuo, J. H. Chang, J. M. Yeh, and W. H. Chan. *Toxicol. Lett.* 197, 8 (**2010**).
35. S. Hackenberg, A. Scherzed, M. Kessler, S. Hummel, A. Technau, K. Froelich, C. Ginzkey, C. Koehler, R. Hagen, and N. Kleinsasser, *Toxicol. Lett.* 201, 27 (**2011**).
36. L. Xu, L. Chen, Z, Dong, J. Wang, Z. Wang, and A. Shao, *Chi. J. Pharm. Anal.* 2, 33 (**2012**).
37. V. C. Sanchez, J. R. Pietruska, N. R. Miselis, R. H. Hurt, and A. B. Kane, *Wiley Interdiscip. Rev. Nanomed. Nanobiotechnol.* 1, 511 (**2009**).

Received: 6 February 2012. Accepted: 7 November 2012.

RESEARCH ARTICLE

Nanoscale   RSCPublishing

PAPER

Challenge to assess the toxic contribution of metal cation released from nanomaterials for nanotoxicology – the case of ZnO nanoparticles†

Cite this: *Nanoscale*, 2013, **5**, 4763

Mingsheng Xu,*[a] Jie Li,[b] Nobutaka Hanagata,[b] Huanxing Su,[c] Hongzheng Chen[a] and Daisuke Fujita[d]

Received 23rd December 2012
Accepted 17th March 2013

DOI: 10.1039/c3nr34251d

www.rsc.org/nanoscale

The identification of physicochemical factors that govern toxic effects of nanomaterials (NMs) is important for the safe design and synthesis of NMs. The release of metal cations from NMs in cell culture medium and the role of the metal cations in cytotoxicity are still under dispute. Here, we report that removal of NMs such as ZnO nanoparticles (NPs) by centrifugation, the procedure commonly used for the estimation of released ion concentration in nanotoxicology, was incomplete even at a relative centrifugal force of 150 000 × *g*. In this sense, the Zn concentration in supernatant measured by inductively coupled plasma-mass spectrometry cannot be regarded as the concentration of free Zn^{2+} ions which were released from ZnO NPs in cell culture medium. This suggests the urgent need to develop relevant analytical techniques for nanotoxicology. The toxic contribution of released Zn^{2+} ions to the A549 cell lines was estimated to be only about 10%. We conclude that the cytotoxicity associated with ZnO NPs is not a function of the Zn concentration, suggesting that other factors play an important role in the toxic effect of ZnO NPs.

1 Introduction

Novel nanomaterials (NMs) are playing key roles in nanotechnology innovations. However, the increasing use of NMs in industrial and consumer products has aroused global concern regarding their potential impact on the environment, human health, and society (NanoEHS). A number of studies on the effects of NMs in *in vitro* and *in vivo* systems have been published,[1,2] and showed that NMs including carbon nanotubes, fullerenes, quantum dots[3] such as CdS, oxide nanoparticles (NPs) such as ZnO, CuO and TiO_2, exhibited various toxic effects on biological systems. Despite the rapid growth of publications associated with NanoEHS recently, there are still many challenges and issues,[4,5] in particular on identifying toxic origins. The identification of physicochemical factors that govern the toxic effects of NMs is important for the safe design and synthesis of NMs and their applications. NMs do not behave in solution as inert objects or soluble small molecules. They often undergo aggregation or agglomeration,[6,7] dissolution processes,[8] and/or adsorption of proteins[9] or ions[10] from biological environments, leading to the formation of new entities.[10]

Many studies had attributed the toxic effects of metal-based NPs (NPs) primarily to released metal cations.[11] For example, Zn^{2+} ions were assumed to be released from ZnO particles as they were dispersed into cell culture medium or outside cells.[8,12–14] It was reported that the dissolution of ZnO NPs could occur in culture medium and reach >80% of the maximum total concentration of dissolved Zn^{2+} ions within 3 h; cell cultures were thus exposed mainly to aqueous Zn^{2+} ions when less than maximum concentrations of ZnO NPs were used.[8] Consequently, the toxic effect of ZnO NPs was mainly attributed to the dissolved Zn^{2+} ions in the cell culture medium.[8,11] By contrast, it was demonstrated that ZnO nanowires were comparatively stable in extracellular medium (pH = 7.4) and dissolution was low.[15] It was also confirmed by Gilbert *et al.*[16] that the majority of ZnO NPs did not dissolve in bronchial epithelial growth medium (BEGM). Furthermore, it was clearly shown that the toxicity of ZnO NPs to human colon-derived RKO cells was independent of the amount of soluble Zn^{2+} ions in the cell culture medium.[17] In the case of CuO NPs, there are also contradicting reports of the contribution of released Cu^{2+} to the observed toxicity.[18,19] The adverse biological effects of CuO NMs were explained by their solubility[20] based on the data obtained by the measurement using inductively coupled plasma-mass

[a]*State Key Laboratory of Silicon Materials, MOE Key Laboratory of Macromolecular Synthesis and Functionalization, Department of Polymer Science and Engineering, Zhejiang University, Hangzhou 310027, P. R. China. E-mail: msxu@zju.edu.cn*
[b]*Interdisciplinary Laboratory for Nanoscale Science and Technology, National Institute for Materials Science, 1-2-1 Sengen, Tsukuba, Ibaraki 305-0047, Japan*
[c]*State Key Laboratory of Quality Research in Chinese Medicine, Institute of Chinese Medical Sciences, University of Macau, Macau SAR, China*
[d]*Advanced Key Technologies Research Division, Nano Characterization Unit, National Institute for Materials Science, 1-2-1 Sengen, Tsukuba, Ibaraki 305-0047, Japan*

† Electronic supplementary information (ESI) available: High-resolution TEM images of ZnO NPs observed in the collected supernatant, TEM image and EDS maps of DMEM with FBS, in which no ZnO NPs were dispersed, XRD pattern for ZnO NPs, hydrodynamic size of ZnO suspensions and supernatants collected from the suspensions. See DOI: 10.1039/c3nr34251d

spectrometry (ICP-MS) relevant techniques or by the simple comparable toxicity to Cu salts[19,21] such as $CuSO_4$. By contrast, it was reported that cytotoxic effects related to the released copper fraction were found to be significantly lower than the effects related to CuO particles.[22,23] Thus, the link of free metal cations liberated from NPs to the observed toxicity or the toxic origin of NPs remains unclear.[19] In all these investigations,[8,12–14,19,20,22–24] the "free ion concentration" was commonly determined by using ICP-MS relevant techniques[25,26] to measure the supernatant collected after the nanomaterial suspension was centrifuged (Fig. 1). However, no study had addressed an important question – can centrifugation completely remove non-dissolved NMs from the suspension? The absence of an analytical technique for measuring the released metallic ion concentration makes it challenging to address the toxic contribution of released metal cations from NMs.

Here, we investigate the effectiveness of centrifugation on the removal of NMs from cell culture medium and the resultant impact on both the estimation of metal cation concentration and its toxic contribution. Our results show that the centrifugation process was unable to completely remove NPs even at very harsh centrifugation conditions, and thus it is not suitable to assume the elemental concentration measured by ICP-MS relevant techniques as the free ions in the suspension of NPs. Our study shows that the cytotoxicity associated with ZnO NPs is not a function of the Zn concentration. The estimated toxic contribution of released Zn^{2+} ions to the A549 cell line is only about 10%. These results shed light on how to evaluate metal cations released from NPs in cell culture medium and its contribution to cytotoxicity.

2 Materials and methods

2.1 Nanoparticles

High-purity ZnO and Al-doped ZnO (elemental Al content of about 3.4%) NPs were obtained from Sigma-Aldrich (Sigma-Aldrich Co., Japan). The primary dimensions and sizes of the oxides were provided in the data sheet, as determined by X-ray diffraction (XRD) and Brunauer–Emmett–Teller (BET) analysis. The average primary sizes of the ZnO and Al-doped ZnO NPs were about 60 nm and 50 nm, respectively, but were not uniform, as previously observed by electron microscopy.[27] We characterized the primary size, shape, and composition of the NPs by scanning electron microscopy (SEM) equipped with energy dispersive spectroscopy (EDS) (JSM-7001F, JEOL Inc., Japan) and by X-ray photoelectron spectroscopy (XPS) (PHI Quantera SXM, ULVAC-PHI, Japan).[27] We also used ZnO NPs with average size of about 20 nm for a comparative study. If not specifically stated, the ZnO NPs in this article are the ZnO NPs with average size of about 60 nm.

2.2 Nanoparticle suspension preparation

The cell culture medium was high-glucose Dulbecco's modified Eagle's medium (DMEM) (pH = 7.4) (Invitrogen) supplemented with 100 units mL^{-1} penicillin and 100 μg mL^{-1} streptomycin, which is simply called as DMEM in the present work. ZnO and Al-doped ZnO NPs were dispersed in the DMEM with or without 10% (v/v) fetal bovine serum (FBS) (SAFC Bioscience Inc.). The concentration of the NP suspensions was 25 μg mL^{-1} or 50 μg mL^{-1}.

2.3 Centrifugation process

The centrifugation of NP suspensions was carried out at 20 000 × *g* or 150 000 × *g* for different periods of time using the Optima LE-80 K Ultracentrifuge (Beckman Coulter, Brea, CA, USA). After centrifugation, the supernatant was collected carefully for use.

2.4 Transmission electron microscopy

The dark-field TEM images, high-resolution TEM (HRTEM) images, elemental mapping, and EDS spectra were analyzed using a JEM-2100F high-resolution transmission electron microscope (JEOL Inc., Japan) with an acceleration voltage of 200 kV.[10] The samples for TEM observation were prepared by immersing a TEM mesh into the supernatant collected after centrifugation of the suspension of ZnO NPs (25 μg mL^{-1}) for 24 h at 37 °C in the dark with 5% CO_2, that is, the same environment as for cell culture. After being dried in air, the TEM mesh was observed. We also carried out control experiments where TEM mesh was immersed into medium with FBS but without ZnO NPs (see ESI, Fig. S1 and S2†).

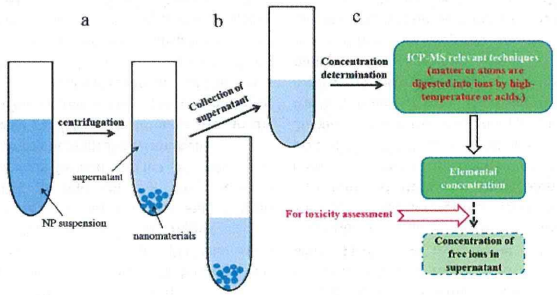

Fig. 1 Schematic diagram showing procedures to measure elemental concentration for toxicity evaluation of the contribution of free metal ions. (a) Centrifugation of nanomaterial suspension. (b) Collection of supernatant for ICP-MS measurement. (c) Measurement of elemental concentration by ICP-MS, and assuming the elemental concentration as the concentration of free ions in the supernatant.

2.5 Hydrodynamic size distribution

The dynamic size of the ZnO (25 μg mL^{-1}) in DMEM with or without FBS and the collected supernatants was measured using a dynamic light scattering spectrophotometer (DLS-6000 AL; Otsuka Electronics, Japan). The DLS data indicate whether or not the suspensions or supernatants contain NPs. For a comparison, no particle was detected in the control sample of the medium with FBS, which suggests that the proteins in the solution did not form sediments under the experimental conditions. All the samples were measured at room temperature and were not incubated at 37 °C in the dark with 5% CO_2 prior to the characterization. This is different from the preparation of samples for TEM characterization because we found that the incubation of cell culture media with FBS in the culture environment leads to formation of particle-shaped matter[10] and in turn influences the DLS analysis. We had no intention to measure the accurate size distribution of the ZnO in these solutions by the DLS technique.

2.6 Elemental Zn concentration

The concentration of elemental Zn in the collected supernatants, ZnO suspensions, and Al-doped ZnO suspensions was measured by using inductively coupled plasma-optical emission spectrometry (SPS1700HVR, Seiko Instruments Inc., Japan). Before the measurements, 10% solutions of the samples were prepared with de-ionized water. The wavelengths used for Zn and Al analysis were 213.9 nm and 396.3 nm, respectively. The provided data were averaged from 3 measurements.

2.7 Viability of the A549 cell line

A549 cell lines were cultured in DMEM with or without FBS and grown in the dark at 37 °C in a 5% CO_2 humidified environment. Cells were seeded into a 3.9 cm^2 dish with a density of about 11 000 cells per cm^2. The cells were allowed to adhere for 24 h, followed by dilution of freshly dispersed nano-oxide suspensions (in sterilized, de-ionized water) into DMEM with or without FBS. After centrifugation of the ZnO suspension at 20 000 × *g* for 20 min, the supernatants were collected and immediately applied to the cells by replacing the old medium after dispersing for approximately 1 min using an Ecan Tube-Mixer (TM-2000, Asahi Techno Glass, Chiba, Japan). In the absence of ZnO NPs, control cells were cultured in the same volume of medium with or without FBS. The concentration dependence of ZnO NP suspensions on A549 cell viability was also investigated.

A calcein-AM staining kit (Dojindo Molecular Technologies Inc., Japan) was used to stain viable cells to assess A549 viability[27] after 24 h exposure to ZnO suspensions and supernatants. Before staining, the cells were washed twice with PBS. After staining, the cells were placed in an incubator for 10 min. Fluorescence images were then acquired using an inverted fluorescence microscope (DM2500 Fluo/PH, Leica Microsystems, Germany). We analyzed at least eight fields of cells in each dish, and used the averages of the data. Each experiment was carried out independently in triplicate. For statistical analysis, a two-tailed Student's *t*-test was performed. The result of this test was expressed as relative cell viability, which was calculated by [test]/[control], and the mean ± SEM (standard error of the mean) of three independent experiments. Results were considered statistically significant at $p < 0.05$.

3 Results and discussion

3.1 Supernatant containing ZnO NPs

Previously, we had characterized the NPs dispersed in different solvents in details;[27] and we found that the NPs can selectively adsorb various components from biological environments and in turn form bio-nanoparticle complexes.[10] Here, we use high-resolution TEM and ICP-OES to determine whether centrifugation can completely remove non-dissolved ZnO NPs from cell culture medium. Fig. 2 shows typical TEM images of the supernatant of ZnO NPs dispersed in DMEM with FBS collected after centrifugation at 20 000 × *g* for 20 min. We also carried out control experiments where a TEM mesh was immersed into DMEM with FBS but without ZnO NPs (see ESI, Fig. S1 and S2†).

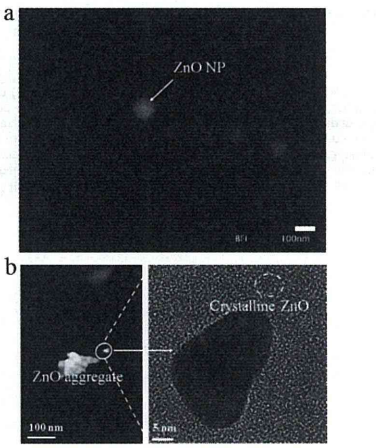

Fig. 2 ZnO NPs remained in the supernatant. (a) Dark-field TEM image. (b) Dark-field low magnification TEM image and high-resolution TEM images. The images were obtained from supernatant collected after centrifugation of the ZnO suspension in medium with fetal bovine serum, showing that crystalline ZnO is observed not only at the core region, but also in the shell region. The results suggest that centrifugation cannot completely remove the NPs from the suspensions.